frontiers in Bioengineering and Biotechnology

ORIGINAL RESEARCH
published: 18 August 2020
doi: 10.3389/fbioe.2020.00931

# A Modular Microscale Granuloma Model for Immune-Microenvironment Signaling Studies *in vitro*

*Samuel B. Berry[1], Maia S. Gower[1], Xiaojing Su[1], Chetan Seshadri[2] and Ashleigh B. Theberge[1,3]**

[1] Department of Chemistry, University of Washington, Seattle, WA, United States, [2] Department of Medicine, University of Washington, Seattle, WA, United States, [3] Department of Urology, University of Washington, Seattle, WA, United States

Tuberculosis (TB) is one of the most potent infectious diseases in the world, causing more deaths than any other single infectious agent. TB infection is caused by inhalation of *Mycobacterium tuberculosis* (Mtb) and subsequent phagocytosis and migration into the lung tissue by innate immune cells (e.g., alveolar macrophages, neutrophils, and dendritic cells), resulting in the formation of a fused mass of immune cells known as the granuloma. Considered the pathological hallmark of TB, the granuloma is a complex microenvironment that is crucial for pathogen containment as well as pathogen survival. Disruption of the delicate granuloma microenvironment *via* numerous stimuli, such as variations in cytokine secretions, nutrient availability, and the makeup of immune cell population, can lead to an active infection. Herein, we present a novel *in vitro* model to examine the soluble factor signaling between a mycobacterial infection and its surrounding environment. Adapting a newly developed suspended microfluidic platform, known as Stacks, we established a modular microscale infection model containing human immune cells and a model mycobacterial strain that can easily integrate with different microenvironmental cues through simple spatial and temporal "stacking" of each module of the platform. We validate the establishment of suspended microscale (4 μL) infection cultures that secrete increased levels of proinflammatory factors IL-6, VEGF, and TNFα upon infection and form 3D aggregates (granuloma model) encapsulating the mycobacteria. As a proof of concept to demonstrate the capability of our platform to examine soluble factor signaling, we cocultured an *in vitro* angiogenesis model with the granuloma model and quantified morphology changes in endothelial structures as a result of culture conditions ($P < 0.05$ when comparing infected vs. uninfected coculture systems). We envision our modular *in vitro* granuloma model can be further expanded and adapted for studies focusing on the complex interplay between granulomatous structures and their surrounding microenvironment, as well as a complementary tool to augment *in vivo* signaling and mechanistic studies.

**Keywords: *in vitro* granuloma model, open microfluidics, immune signaling, paracrine signaling, microenvironment, modular**

OPEN ACCESS

***Edited by:***
*Nuno M. Neves, University of Minho, Portugal*

***Reviewed by:***
*Fransisca Leonard, Houston Methodist Research Institute, United States*
*Luciana Dini, Sapienza University of Rome, Italy*

***Correspondence:**
*Ashleigh B. Theberge*
*Abt1@uw.edu*

***Specialty section:***
*This article was submitted to Nanobiotechnology, a section of the journal Frontiers in Bioengineering and Biotechnology*

***Received:*** *14 April 2020*
***Accepted:*** *20 July 2020*
***Published:*** *18 August 2020*

***Citation:***
*Berry SB, Gower MS, Su X, Seshadri C and Theberge AB (2020) A Modular Microscale Granuloma Model for Immune-Microenvironment Signaling Studies in vitro. Front. Bioeng. Biotechnol. 8:931. doi: 10.3389/fbioe.2020.00931*

## INTRODUCTION

Tuberculosis (TB) is one of the most potent infectious diseases in the world, causing more deaths than any other single infectious agent (World Health Organization, 2019). TB infection is caused by inhalation of *Mycobacterium tuberculosis* (Mtb) and subsequent phagocytosis and migration into underlying lung tissue and the lymph system by responding immune cells (e.g., alveolar macrophages and dendritic cells) (Kaufmann, 2004; Saunders and Britton, 2007). Due to the inability of these innate immune cells to clear Mtb, persistent Mtb induce an adaptive immune response, leading to the formulation of a fused mass of immune cells around Mtb known as a granuloma (Saunders and Britton, 2007). Within the granuloma, Mtb typically enter a latent phase characterized by a non-proliferative phenotype and lipid uptake (Peyron et al., 2008; Deb et al., 2009; Russell et al., 2009), leading to a latent infection that is effectively contained (World Health Organization, 2019). However, disruption of the delicate equilibrium between proinflammatory factors [e.g., tumor necrosis factor-α (TNFα), interferon-γ (IFNγ)], microenvironment conditions (e.g., hypoxia and pH), and immune cell populations (e.g., macrophages and T cells) can lead to reactivation of latent Mtb and deterioration of the granuloma, initiating an active TB infection and dissemination of infectious mycobacteria (Russell et al., 2009; Ramakrishnan, 2012).

Deciphering the impact of microenvironment variations around the granuloma remains a significant challenge, and researchers often rely on *in vivo* animal models or biological samples (e.g., blood and tissue biopsy), considered the gold standard for studying TB, to reconstruct this complex environment. These methods have laid the foundation for understanding the pathogenesis and immunology behind TB, yet many existing *in vivo* models do not accurately recapitulate Mtb infection as seen in humans (although recent advances in mouse models and the established zebrafish/*M. marinum* model are closing this gap) (Cronan and Tobin, 2014; Myllymäki et al., 2016; Gern et al., 2017; Zhan et al., 2017; Cronan et al., 2018; Yong et al., 2018). Additionally, despite recreating the complexity of an *in vivo* environment, spatial manipulation and probing of the granuloma microenvironment through introduction or removal of immune and tissue components is difficult in most animal models (Scanga and Flynn, 2014; Foreman et al., 2017; Zhan et al., 2017). Further, human-derived biological samples provide detailed cellular information regarding the granuloma, the immune response, and disease status (Guyot-Revol et al., 2006; Berry et al., 2010; Darboe et al., 2019; Ogongo et al., 2020), but are inherently limited as they only reflect a singular point in time, rather than the dynamic interactions that occur during the early stages of infection or disease progression.

Alternatively, researchers have utilized *in vitro* models to examine specific processes and immune phenomena associated with TB infection and granuloma formation, augmenting the valuable information elucidated from *in vivo* models (Birkness et al., 2007; Peyron et al., 2008; Deb et al., 2009; Kapoor et al., 2013; Elkington et al., 2019). These models, which often rely on infection of patient-derived peripheral blood mononuclear cells (PBMCs) with mycobacterial strains, have successfully mimicked granuloma formation and behavior through soluble factor signaling between immune cells (Puissegur et al., 2004; Birkness et al., 2007; Crouser et al., 2017), Mtb reactivation (Kapoor et al., 2013), and PBMC differentiation (Peyron et al., 2008). However, many of these *in vitro* models consist of granulomas grown inside of well plates (Puissegur et al., 2004; Birkness et al., 2007; Peyron et al., 2008; Kapoor et al., 2013; Crouser et al., 2017), limiting the ability of the researchers to easily manipulate the microenvironment of the granulomas and increase the complexity of their granuloma models through multiculture and introduction of key components of the microenvironment on demand. Recently, more complex, biomimetic models have been developed that have successfully recapitulated important biological phenomena (Parasa et al., 2014, 2017) and examined novel therapeutic approaches to combat TB infection (Bielecka et al., 2017; Tezera et al., 2017), while simultaneously demonstrating innovative and tractable platforms. However, these models face limitations in studies where users wish to subject granulomas to various microenvironmental cues over time, or in enabling the addition of tissue components after the model is established.

Building upon the foundation created by previous *in vitro* models, we present the creation of a novel microscale *in vitro* granuloma model that can be adapted to study the soluble factor signaling between granulomas and their surrounding microenvironment immediately following infection. Using a recently developed modular microfluidic coculture platform, known as "Stacks"(Yu et al., 2019), we demonstrate a multi-layered coculture that can be spatially and temporally manipulated to mimic different microenvironments and timepoints. The Stacks platform utilizes suspended cultures, wherein a droplet is contained in a well consisting of walls but lacking a ceiling or floor (Casavant et al., 2013; Humayun et al., 2018; Berthier et al., 2019), thereby enabling users to vertically stack layers containing different cell types and place them in signaling contact (Yu et al., 2019). The modular component of the Stacks, as well as of other microfluidic platforms, offers a notable advantage as users can optimize model conditions individually and connect each component to create different complex systems (Ong et al., 2019; Yu et al., 2019). As a proof of concept, we use a model mycobacterial strain known to induce granuloma formation *in vitro* (Seitzer and Gerdes, 2003; Puissegur et al., 2004), *Mycobacterium bovis* Bacillus Calmette- Guérin (BCG), with human blood-derived immune cells and validate its ability to form an *in vitro* granuloma model on the microscale (4 μL culture volume) in a layer of the Stacks platform. Further, to demonstrate the ability of our stackable microscale infection model to signal with its surrounding microenvironment in a proof-of-concept system, we miniaturize an existing *in vitro* angiogenesis model (containing primary human endothelial cells) within a separate stackable layer (Koh et al., 2008; Lonza, 2018; Yu et al., 2019). Here, we validate the development of our microscale *in vitro* granuloma model and demonstrate the capability of the system to support soluble factor signaling between the granuloma model and a separate stackable endothelial culture. We envision our modular *in vitro* granuloma model can be further developed to

include additional layers of immune cells, tissue models, and pathogens for studies examining the complex interplay between granulomatous structures and their surrounding environment, as well as a complementary tool to augment *in vivo* signaling and mechanistic studies.

# RESULTS AND DISCUSSION

## Microscale Granuloma Model Design and Overview

We present a modular *in vitro* platform that we adapted to enable the ability to add, modify, and manipulate the granuloma microenvironment for studying the effects of cellular signaling on granuloma formation and development. To create this *in vitro* model, we adapted a previously described open microfluidic platform ["Stacks"(Yu et al., 2019; **Figure 1**)] that relies on key fluidic principles, namely capillary pinning, to enable vertical stacking and removal of discrete cell culture wells without leakage or horizontal flow between stacked layers. The pinning of fluids within this platform is vital to contain cultures within the open wells and allows for the connection and separation of the wells without bonding or disruption of the cultures, respectively. Additionally, the Stacks platform provides numerous advantages such as pipette accessibility (due to its open culture wells), bio- and imaging compatibility (due to its fabrication from polystyrene or polypropylene), and microscale culture wells. Further, the Stacks device relies on surface tension and capillary forces for functionality, removing the need for external pumps commonly associated with microfluidic chips (i.e., syringe pumps) and allowing it to fit within common cell culture materials (e.g., OmniTray$^{TM}$, petri dish) and incubators. For our *in vitro* model system, we created an independent layer that can be clicked together with other layers containing culture models to initiate paracrine signaling or separated for independent analysis, thereby allowing us to temporally introduce different signaling microenvironments to our *in vitro* granuloma model (**Figure 1**; Yu et al., 2019). This Stacks layer, herein called the granuloma layer, consists of an infection model of human monocyte-derived macrophages (MDMs) and a model mycobacterium strain, *Mycobacterium bovis* Bacillus Calmette-Guérin (BCG), suspended in a 3D extracellular matrix (ECM) plug to mimic some aspects of *in vivo* granuloma behavior (e.g., pathogen encapsulation, soluble factor secretion, aggregate formation) previously observed in other *in vitro* granuloma models (Birkness et al., 2007; Kapoor et al., 2013; Crouser et al., 2017).

Previous *in vitro* granuloma models successfully recapitulated important components of granulomatous infections including leukocyte recruitment and signaling, establishment of dormancy and resuscitation, and genetic diversity at scales ranging from 12 well plates to 96 well plates (Birkness et al., 2007; Kapoor et al., 2013; Crouser et al., 2017). Our model adds to these existing techniques through miniaturization and introduction of modularity to enable examination of the signaling phenomena between a mycobacterial infection and its surrounding microenvironment. We reduce the volume of our cultures (4 μL/well) more than 10-fold from previous examples (50–500 μL/well) to decrease cell and reagent usage in our model; further, we mix BCG and MDMs together in a 3D extracellular matrix (ECM), without pre-infecting the MDMs, to establish the infection in our granuloma layer after a minimum of 24 h (**Figure 1**). However, due to the scale of the model (4 μL/well), the media buffering capacity, nutrient availability, waste accumulation, and multiplicity of infection (MOI) all needed to be optimized to permit successful formation of the granuloma layer (**Supplementary Information 2**). This is consistent with prior investigations on the effects of miniaturization on mammalian cell cultures (Su et al., 2013).

## Validation of Granuloma Model in Stacks Platform

To validate the successful establishment of a microscale *in vitro* granuloma model within our platform, we used three separate previously reported readouts: (1) aggregate formation, (2) encapsulation of the mycobacterium within host immune cells, and (3) soluble factor analysis (Birkness et al., 2007; Kapoor et al., 2013; Crouser et al., 2017; Tezera et al., 2017). After initiating infection by mixing MDMs and BCG into the ECM (collagen I) and seeding it into the wells, we consistently observed aggregate formation in the granuloma layer containing BCG when wells were fixed and imaged on Day 4 post infection (p.i.) (**Figure 2**, **Supplementary Figure 3**, and **Supplementary Table 1**). Using mCherry-expressing BCG, we observed aggregation of CellTracker Green-stained MDMs around the BCG in infection wells, whereas little to no aggregate formation was observed in the uninfected control wells (**Figure 2**); the 3D structure of the aggregates containing MDMs and BCG was confirmed through confocal imaging of the granuloma layers on Day 4 p.i. (**Figure 2**). We observed complete encapsulation of BCG within the multi-cellular aggregate, oftentimes noting the presence of multiple spatially distinct BCG within one aggregate and little to no extracellular BCG (**Figure 2**). An advantage of mixing the BCG and MDMs without direct pre-infection of the MDMs is that MDMs must sample and migrate through the 3D collagen matrix in order to initiate the infection and respond to other infected MDMs, a process which is further supported by the microscale culture wells and an optimized MOI of 0.05. Further, CellTracker Green staining of the MDMs enables live cell imaging of these multicellular aggregates (no fixation and additional preparation steps required), as the dye stains live cells and is retained intracellularly (**Supplementary Figure 3**).

To illustrate the capability of our model to be used for soluble factor signaling studies, we analyzed the secretion profile of three granuloma-associated proinflammatory factors: interleukin-6 (IL-6), tumor necrosis factor α (TNFα), and vascular endothelial growth factor (VEGF) (**Figure 3**) from the model granuloma layer (in monoculture) (Lin et al., 2007; Martinez et al., 2013; Singh and Goyal, 2013; Polena et al., 2016). In accordance with previous models and studies (Birkness et al., 2007; Lin et al., 2007; Martinez et al., 2013; Singh and Goyal, 2013; Polena et al., 2016) we observed significantly greater secretion of IL-6 ($P$ = 0.005) and VEGF ($P$ = 0.039) in our infected granuloma layers (+BCG) when compared to

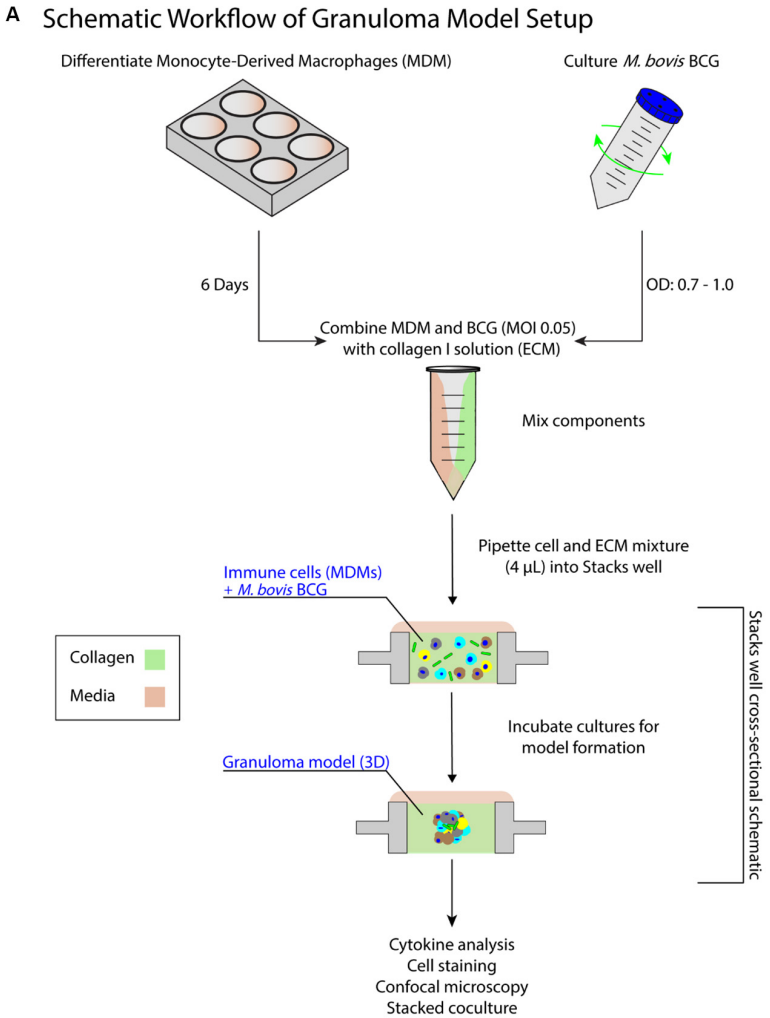


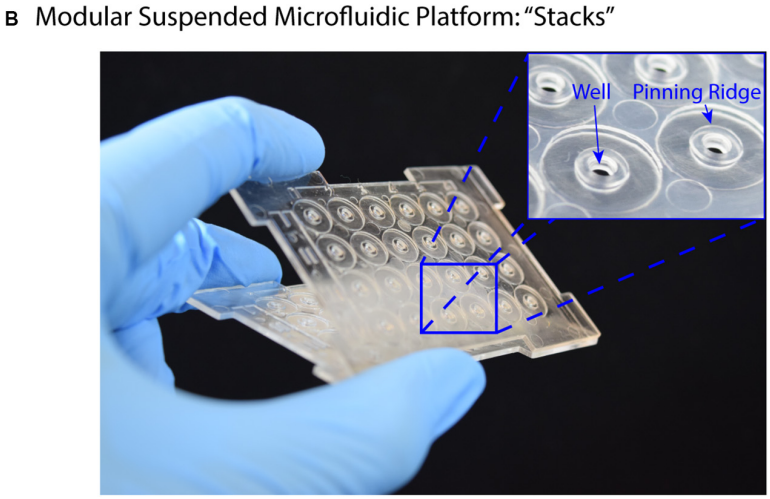


**FIGURE 1 |** Suspended open microfluidic platform enables creation of a modular *in vitro* granuloma model. **(A)** Schematic workflow showing setup and establishment of the model granuloma layer in the Stacks platform. Once established, the model granuloma layer can be stacked with other layers to initiate coculture paracrine signaling. **(B)** The "Stacks" platform (Yu et al., 2019) contains an array of 24 individual suspended wells to facilitate the exchange of signals through the top and bottom of the well to neighboring layers and can be easily combined and removed. The inset illustrates the open suspended wells (2 mm diameter) and pinning ridges required to prevent leakage within the platform.

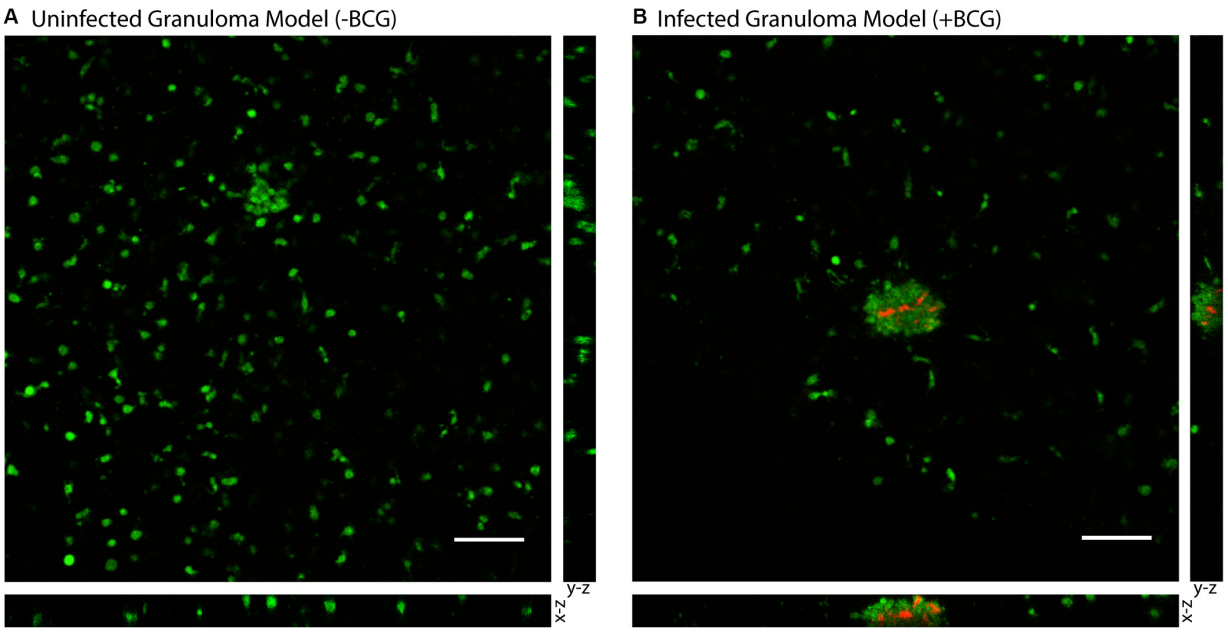


**FIGURE 2 |** Aggregation of *M. bovis* BCG and MDMs in 3D collagen plugs within a layer of the Stacks microscale culture system. **(A)** CellTracker Green-stained MDMs remain dispersed in a 3D collagen plug in the absence of coincubation with BCG. **(B)** MDMs encapsulate mCherry-expressing BCG in the granuloma layer and form large multicellular aggregates that surround the BCG-infected MDMs and contain the mycobacterium within the aggregate. Confocal microscopy shows the structure of the aggregated MDMs with BCG and illustrates containment of the BCG within the aggregate of MDMs in the suspended 3D collagen plug. Representative images obtained on Day 4 p.i. MOI: 0.05. Scale bar: 100 μm. Bottom image depicts *x-z* plane (66.5 μm thickness) and right image depicts *y-z* plane (66.5 μm thickness).

our control layers containing uninfected MDMs in monoculture (−BCG); further, we observed a 5–17-fold increase in TNFα secretion in 3 out of 4 independent experiments under the same conditions and a strong trend toward greater TNFα secretion (**Figure 3** and **Supplementary Figure 4**). We also observed decreasing secretion of IL-6, TNFα, and VEGF over 5 days, with the greatest concentrations observed for IL-6 and TNFα on Day 1 and for VEGF on Day 2 (**Figure 3** and **Supplementary Figure 4**). These results indicate that our platform is able to exhibit infection-dependent increases in soluble factor secretion, wherein there is a large burst of proinflammatory factors immediately following infection, that then decreases and stabilizes over time as we begin to observe aggregate formation in the granuloma layers. Additionally, while we observe the anticipated increases in the secretion of these factors, we would expect a more robust response if more virulent strains than BCG were used, as increased secretion of factors has been observed with infection by more virulent mycobacterial strains (Engele et al., 2002; Polena et al., 2016). In this work, we selected IL-6, VEGF, and TNFα as well-established cytokines to validate the secretion profile of our model (Birkness et al., 2007; Kapoor et al., 2013; Domingo-Gonzalez et al., 2016; Polena et al., 2016; Crouser et al., 2017); in particular, we included factors relevant for angiogenesis (i.e., VEGF) to validate its use in vasculature coculture models. Importantly, many other customizable combinations of signaling molecules can be analyzed depending on the biological question of interest, further supporting the use of this model granuloma layer for different biological assays. Thus, these results support the use of our microscale granuloma model for studies of soluble factor signaling involving the granuloma layer, and its broader use for mycobacterial infection cytokine studies (Domingo-Gonzalez et al., 2016).

## BCG Granulomas Modulate Endothelial Structure Morphology *in vitro*

As a proof of concept to demonstrate the use of our microscale granuloma model in the Stacks platform, we developed a coculture system containing an established angiogenesis model (Koh et al., 2008; Sarkanen et al., 2011; Theberge et al., 2015; Lonza, 2018; Yu et al., 2019) that can be used to probe granuloma-associated angiogenesis (Datta et al., 2015; Oehlers et al., 2015; Osherov and Ben-Ami, 2016; Polena et al., 2016). Mycobacterium-mediated angiogenic processes and granuloma vascularization result from the secretion of proangiogenic factors by the infected immune cells that compose the granuloma and play a complex and evolving role during the course of infection (Oehlers et al., 2015, 2017; Polena et al., 2016; Torraca et al., 2017). Extensive work has been conducted on understanding the role of angiogenesis in granuloma outcome, finding that inhibition of VEGF and other signaling pathways reduces pathogenicity and dissemination of infectious mycobacteria (Oehlers et al., 2015; Polena et al., 2016; Harding et al., 2019) while normalizing surrounding vasculature, improving small molecule delivery, and decreasing hypoxia within the granuloma

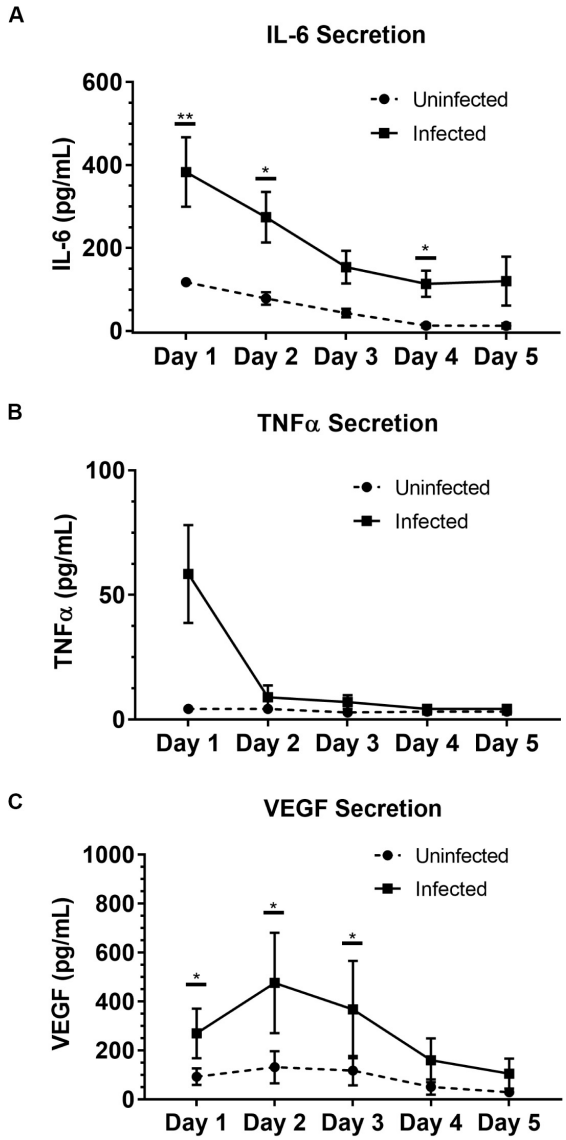


**FIGURE 3 |** Soluble factor analysis of granuloma layer supernatants illustrates proinflammatory profile of infection model. Infection with BCG causes significant increases in secretion of **(A)** IL-6 and **(C)** VEGF in the Stacks platform, and shows an increasing trend in **(B)** TNFα secretion Day 1 p.i. Secretion of IL-6, TNFα, and VEGF decreases over time in infected granuloma layers following infection, corresponding with the formation of aggregates starting around Day 3 p.i. For Day 1–5 p.i., media was replaced daily and supernatant collected from each day was analyzed. Each point represents pooled supernatant samples from 24 technical replicates from $n = 4$ independent experiments. Error bars: SEM. $^{*}P < 0.05$; $^{**}P < 0.01$; Ratio paired *t*-test. Results from each independent experiment on each day are provided in **Supplementary Figure 4** for reference.

(Datta et al., 2015). Similarly, we observed increased secretion of VEGF from infected cells within our microscale granuloma model (**Figure 3C**), and therefore sought to illustrate one potential use of our platform as a complimentary tool for studies examining this infection-mediated process.

To establish this granuloma-vasculature model coculture system, we created a second Stacks layer containing a floor, enabling culture of human endothelial cells on a hydrogel plug (Matrigel) while retaining the ability to be placed in soluble factor signaling contact with the granuloma layer. We selected an *in vitro* model of angiogenesis that has been extensively used to screen angiogenic stimulants and inhibitors, wherein human endothelial cells cultured in well plates self-assemble into tubule-like networks and demonstrate cell sprouting and branching (Bishop et al., 1999; Koh et al., 2008; Sarkanen et al., 2011; Lonza, 2018). To adapt this *in vitro* angiogenesis model into a Stacks layer (herein called the endothelial layer) for use, we miniaturized the established *in vitro* angiogenesis assay (Koh et al., 2008; Lonza, 2018) and seeded it into a separate Stacks layer that could then be subsequently clicked together with the granuloma layer to initiate soluble factor signaling between the two layers (**Figure 4** and **Supplementary Information 3**).

By placing the primary human endothelial cells on a separate Stacks layer, we demonstrate one potential use of our model to examine the induction of angiogenic processes around the granuloma layer and how those angiogenic processes are affected by the soluble factor signaling profile of the granuloma layer in a proof of concept system. In order to examine the influence of the soluble factor profile from the granuloma layer on the endothelial layer, we independently established the granuloma layer and the endothelial layer under their optimized culture conditions (**Figure 4**); the modularity of the Stacks platform enables both layers to be cultured in their optimal conditions (and in separate incubators) without risk of cross contamination prior to joining the layers. The granuloma layers were infected and incubated 24 h prior to clicking with the endothelial layer, and the endothelial layers were seeded 2 h prior to allow the cells to self-assemble into a tubule-like network (Sarkanen et al., 2011; Lonza, 2018). Within this experimental timeframe, we note the absence of large multicellular aggregates within the granuloma layer like those observed on Day 4 p.i., and this is in accordance with our temporal observations (**Supplementary Table 1**). Separate layers were then stacked together and connected by a bridge of shared media to allow passage of factors between the two layers (**Figure 4**). After 16 h of signaling, we separated the layers and fixed, stained, and imaged the vasculature to analyze its morphology as a result of coculture with the granuloma layer (**Figure 5**). We found that after 16 h of coculture, endothelial cells in contact with infected granuloma layers (+BCG) formed thinner, centralized structures with diffuse cell sprouts extending from the center, whereas endothelial cells in contact with uninfected control layers (−BCG) formed wider and larger structures that retained some interconnected networks (**Figure 5**). We quantified these morphological differences through measurement of their tubule index, a metric that measures the ratio of the endothelial structure perimeter to the endothelial structure area and can be used to discern between endothelial structure morphologies (e.g., tubule network, single tubule, and islands/clusters) (Theberge et al., 2015), and found significant morphological differences between endothelial layers cocultured with infected granuloma layers (+BCG) when compared with uninfected granuloma layers (−BCG) (**Figure 5**).

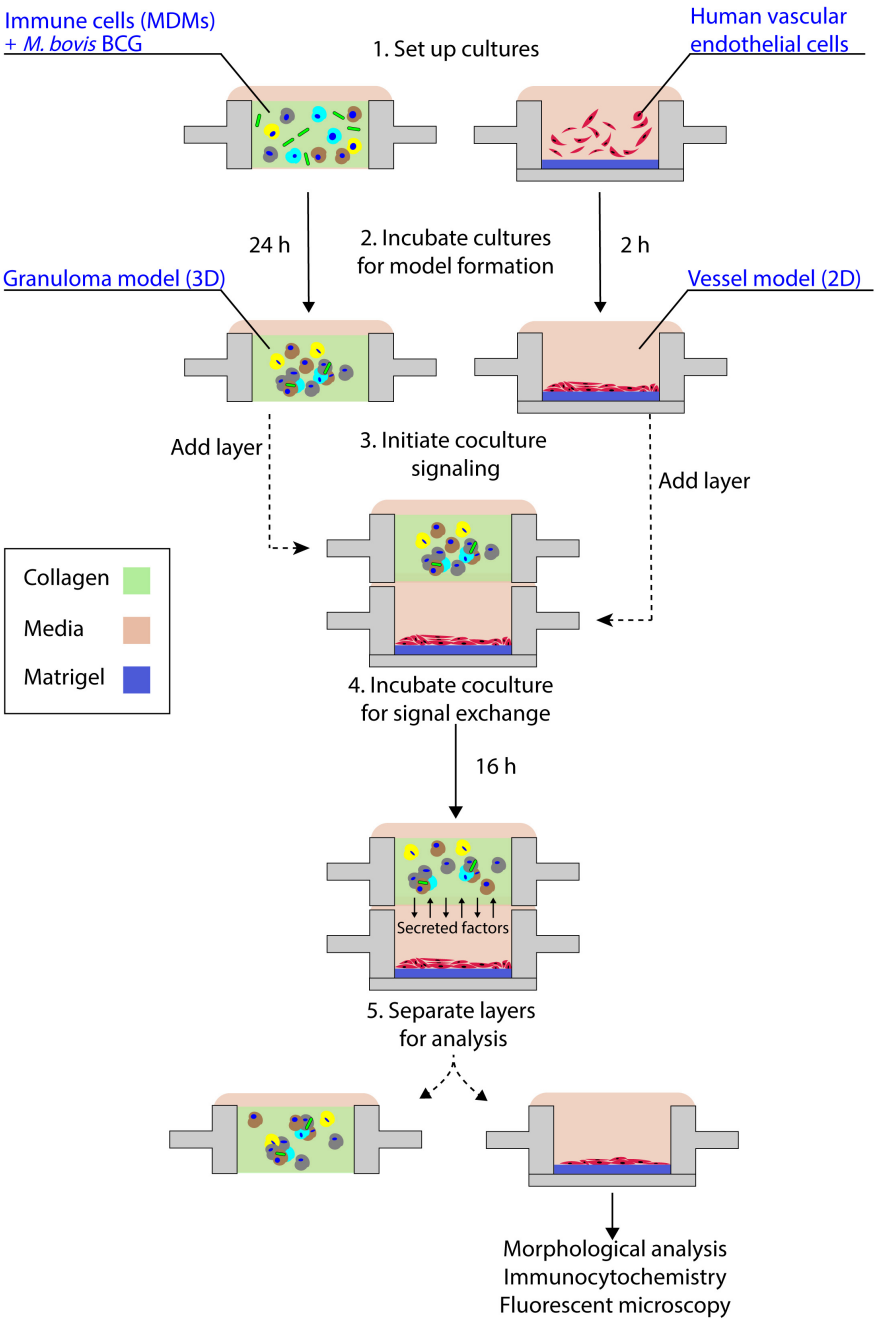


**FIGURE 4 |** Schematic representation of granuloma layer-endothelial layer coculture workflow. The granuloma model layer and the endothelial layer (representing a model microenvironment system) are independently cultured in optimized conditions prior to stacking the layers to initiate soluble factor signaling; after coculture, layers are separated and the morphology of the multicellular endothelial structures is analyzed. For the experimental time points used in this coculture system, we note the absence of large multicellular aggregates within the granuloma model layer, in accordance with our temporal observations (**Supplementary Table 1**).

The morphological change is likely the result of the increased secretion of factors from BCG-infected MDMs, such as VEGF (**Figure 3C**); however, it is possible that additional factors we did not quantify are also contributing to the differences in endothelial morphology. Ultimately, the induction of morphology changes in the endothelial layer as a result of coculture with different model granuloma layers illustrates the ability of the granuloma layer to signal with a neighboring layer representing microenvironmental components.

As we chose to connect the layers at Day 1 p.i. to correlate with increased levels of VEGF and cytokine secretion (**Figure 3**), we expect our model and results would mimic an earlier time point in infection, when the mycobacteria-infected cells are still secreting proinflammatory factors to recruit other immune cells

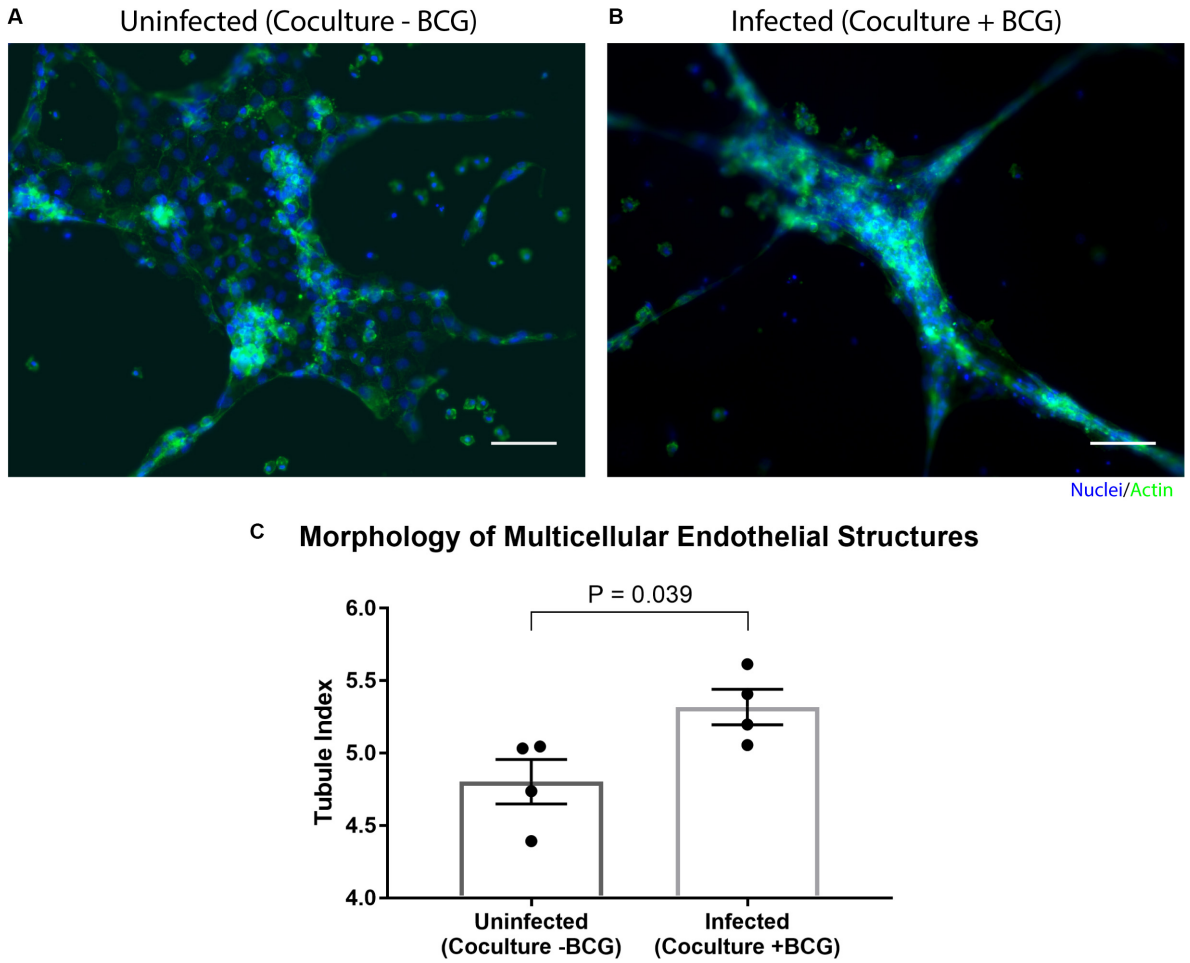


**FIGURE 5 |** Coculture of endothelial layer with granuloma layer impacts morphology of multicellular endothelial structures. Representative images of an endothelial layer cocultured with an uninfected (-BCG) layer **(A)** or infected (+BCG) layer **(B)** for 16 h, illustrating the difference in endothelial morphology as a result of coculture. **(C)** The tubule index (perimeter/area ratio) was used to quantify the morphology of endothelial structures and shows a significant difference between coculture conditions, demonstrating the ability of the model granuloma layer to signal with the endothelial layer. Scale bar: 100 μm. Error bars: SEM. $P < 0.05$, unpaired *t*-test. Each point represents the average ratio of an independent experiment ($n = 4$ independent experiments are plotted).

and the vasculature. Depending on user queries, these layers can also be stacked at more advanced time points (such as from Day 2 p.i. to Day 3 p.i., Day 4 p.i. to Day 5 p.i., and so forth) to study the effect of a later soluble factor profile on the surrounding vasculature, illustrating a key advantage of the modularity of the Stacks system and the flexibility in timing to combine the layers (**Figure 4**). Further, the ability of the model granuloma layer to communicate with the vasculature and modulate the endothelial morphology demonstrates the usage of this platform for signaling studies between our infected granuloma layers and microenvironment components. It is important to note that in our platform, the granuloma layer is not vascularized directly, as is observed *in vivo* (Datta et al., 2015), and that in our system, our endothelial layer is more akin to modeling the surrounding vasculature that is manipulated during early TB infection (Oehlers et al., 2015; Polena et al., 2016). The ability to create two independent layers that are in soluble factor signaling contact enables users to isolate the effects of the soluble factors from the granuloma layer on its surrounding microenvironment without interference from juxtacrine signaling or physical interactions.

## CONCLUSION

Microenvironmental effects, such as soluble factor signaling, play a vital role in granuloma outcome, as the immune system attempts to contain and impede pathogenic mycobacterium from manipulating its environment in favor of its survival (Ramakrishnan, 2012). For example, induction of angiogenic processes by Mtb in the microenvironment surrounding a granuloma have been linked to pro-pathogen outcomes (Oehlers et al., 2015; Osherov and Ben-Ami, 2016), while treatment with anti-angiogenic factors can be a potential treatment option to improve the effects of existing drug regiments (Datta et al., 2015). To further understand the signaling environment and timeline of these phenomena, we created a novel *in vitro* granuloma

model that can be used to study soluble factor signaling between the granuloma and its surrounding microenvironment. As a proof of concept model, we created a two-layered modular microfluidic system containing a mycobacterial infection and an endothelial vasculature model that can be used to compliment *in vivo* granuloma and angiogenesis models (Datta et al., 2015; Oehlers et al., 2015, 2017; Polena et al., 2016). We demonstrate creation of a viable mycobacterial infection using human blood-derived immune cells and BCG within a 4 μL suspended collagen plug, and validate the secretion of proinflammatory cytokines associated with mycobacterial infection. Further, we provide a model coculture system that can be used to probe granuloma-associated angiogenic processes *in vitro*. The modularity and microscale size of our model enables users to add or remove additional cell types at various time points, and to utilize limited cell populations, such as patient cells or rare immune cells, and valuable reagents, such as antibodies or expensive drugs. In this work, we demonstrate the use of the Stacks platform within a system containing predetermined analytical endpoints; however, the modularity of the platform allows users to conduct exploratory studies to examine the effect of the duration or configuration of the Stacked coculture on various biological outputs without predefined time points. Additionally, the design of the platform and fabrication method supports the creation of arrays to test various culture conditions/treatments and customizability to introduce additional functionality (e.g., flow), as well as easy integration with BSL3 laboratory workflows as the device is disposable and fits inside common cell culture materials (e.g., petri dish, OmniTray$^{TM}$, etc.). Further development of our system includes the addition of adaptive immune cells (e.g., T cells) and introduction of parenchymal and stromal cells (e.g., epithelial cells, fibroblasts) to model signaling interactions in the pulmonary environment, probing the soluble factor profile of varied mycobacterial infection signaling phenomena (i.e., expanding the cytokines measured), as well as the use of virulent *M. tuberculosis* to induce more *in vivo*-like responses. Ultimately, we created a tractable and customizable mycobacterial infection model that can be utilized by other researchers to examine the various signaling components of a complex tuberculosis infection.

# MATERIALS AND METHODS

## Stacks Device Fabrication

Stacks devices (Yu et al., 2019) were fabricated from either polypropylene (PP) (granuloma layer) or polystyrene (PS) (endothelial layer) (**Supplementary Figure 1** and **Supplementary Table 1**). PP devices were injection molded (ProtoLabs, Maple Plain, MN, United States) and were flattened using a bench top manual heated press (#4386, Carver Inc., Wabash, IN, United States) for 1 h at 110°C (protocol in **Supplementary Information 1**). After flattening, devices were cleaned with isopropanol (IPA) sonication for 1 h to remove any fabrication residue or contaminants, and then rinsed twice with fresh IPA before drying with compressed air. Prior to use, devices were UV-sterilized for 30 min in a biosafety cabinet. PS devices containing a floor were designed using Fusion360 CAD software (Autodesk, San Rafael, CA, United States) and milled using a Datron Neo CNC mill (Datron Dynamics Inc., Livermore, CA, United States). PS devices and bottoms (floors, 53 mm × 53 mm) were milled from 1.2 mm thick PS sheets (Goodfellow Corp., Coraopolis, PA, United States). To attach the floor to the PS Stacks layer, floors were solvent bonded to the bottom of the Stacks layer using acetonitrile at 75°C for 10 min, followed by 15 min at 75°C to allow excess acetonitrile to evaporate. Solvent-bonded devices were then sonicated in IPA for 80 min and 70% ethanol for 15 min. Devices were then soaked in sterile deionized water for a minimum of 3 h, dried with compressed air, and UV-sterilized for 30 min prior to use. Device holders were designed on Solidworks CAD software (Solidworks Corp., Waltham, MA, United States), converted into G-code using SprutCAM CAM software (SprutCAM, Naberezhnye Chelny, Russia), and milled using a Tormach PCNC Micromill (Tormach Inc., Waunakee, WI, United States). Device holders were fabricated from 4 mm thick PS and were sonicated in IPA for 1 h and UV-sterilized for 30 min prior to use. All device and device holder design files are included in the **Supplementary Table 1**.

To prevent evaporation of microliter volumes of samples, culture platforms were placed in a Nunc Omnitray$^{TM}$ (Thermo Fisher Scientific) which was then placed in a bioassay dish (#240835, Thermo Fisher Scientific) for secondary containment; both the Omnitray and bioassay dish were filled with sacrificial water droplets (1 mL and 5 mL, respectively) to create a humidified environment around the platform, and all cultures were then placed into a water-jacketed incubator.

## Cell Culture

Human peripheral blood mononuclear cells (PBMCs) were isolated from patient whole blood samples (Bloodworks NorthWest, Seattle, WA, United States) using the Ficoll-Paque PLUS media density separation protocol (Thermo Fisher Scientific, Waltham, MA, United States). Briefly, blood samples were diluted with PBS (Thermo Fisher Scientific) and layered atop the Ficoll-Paque. Tubes were then centrifuged for 20 min at 1900 RPM without brakes, and afterward white blood cells at the plasma-Ficoll-Paque interface were collected and resuspended in PBS + 2% fetal bovine serum (FBS, Thermo Fisher Scientific) + 1 mM ethylenediaminetetraacetic acid (EDTA, Gibco, Thermo Fisher Scientific). Cells were then rinsed with subsequent centrifugation (10 min, 500 × *g*) and resuspension until the supernatant was clear. Isolated PBMCs were then cryopreserved in solution containing 90% heat-inactivated FBS (HI-FBS) (Thermo Fisher Scientific) and 10% dimethyl sulfoxide (DMSO) (Sigma-Aldrich, St. Louis, MO, United States) and stored in liquid nitrogen until use. To differentiate the PBMCs into monocyte-derived macrophages (MDMs), PBMCs were thawed and resuspended in serum free RPMI 1640 media (Gibco, Thermo Fisher Scientific); following resuspension, PBMCs were seeded into a 6 well plate (#3516, Corning Inc., Corning, NY, United States) and allowed to incubate for 3 h at 37°C and 5% $CO_2$ for monocyte adhesion. After 3 h, suspended cells were removed, adherent cells were

washed once with 1X phosphate-buffered saline (PBS, Fisher Scientific), and then RPMI 1640 containing 10% HI-FBS, 2 mM L-glutamine, 25 mM HEPES, and 50 ng/mL macrophage colony-stimulating factor (M-CSF) (R&D Systems, Minneapolis, MN, United States) was added to each well. Media was changed on Day 3 and Day 6 post-seeding, and MDMs were used after Day 6. For specific experiments or assays where users require a high purity of cells, we suggest the use of alternative methods, such as light-based or magnetic-activated cell sorting (MACS), to the methods we present here.

mCherry-expressing *M. bovis* Bacillus Calmette-Guérin (BCG) (graciously provided by the Urdahl Lab, Seattle Children's Research Institute, Seattle, WA, United States) was cultured in Middlebrook 7H9 broth (Thermo Fisher Scientific) containing 10% Middlebrook ADC enrichment supplement (Thermo Fisher Scientific), 0.003% Tween-80 (Fisher Scientific), and 50 μg/mL hygromycin B (Sigma-Aldrich). A lower Tween-80 concentration had to be used to ensure that the surfactant did not interfere with the microfluidic media pinning in the Stacks device (**Supplementary Information 2**). BCG was cultured at 37°C and 170 RPM to an OD of 0.7–1.0 for use, passed through a 27G needle to break up aggregates, and diluted to a working concentration for the experiment. BCG was used for all experiments as it can be used within a BSL2 facility, and we did not have access to virulent mycobacterium strains nor a BSL3 facility to perform these experiments.

Human umbilical vein endothelial cells (HUVECs) (Lonza, Basel, Switzerland) were cultured in completed EGM-2 media and maintained at 37°C and 5% $CO_2$ until 80–90% confluence. Passage 5–7 cells were used.

## 3D Granuloma Assay

Monocyte-derived macrophages were differentiated for a minimum of 6 days prior to use, and BCG was grown to an OD of 0.7–1.0 for use. MDMs were rinsed once with 1X PBS and detached with enzyme-free Cell Dissociation Buffer (#13151014, Life Technologies, Thermo Fisher Scientific) at 37°C for 5 min and vigorous pipetting. Detached cells were neutralized with complete RPMI 1640 media, counted, and resuspended at a density of $4 \times 10^7$ cell/mL. BCG was vortexed for 30 s, vigorously mixed via pipetting, and then diluted into 4 mL of complete RPMI 1640 media for a final concentration of $2 \times 10^6$ BCG/mL. An extracellular matrix (ECM) mix containing 80 μL 3 mg/mL type I bovine collagen (Advanced Biomatrix Inc., Carlsbad, CA, United States), 10 μL 10X HEPES buffer, 7 μL deionized $H_2O$, 3 μL 0.5N NaOH, and 2.25 μL 1 mg/mL human fibronectin (Sigma-Aldrich) was mixed and stored on ice until use. To prepare the suspended cell-laden collagen plugs, 25 μL of MDMs (at $4 \times 10^7$ cells/mL) and 25 μL of BCG (at $2 \times 10^6$ BCG/mL) or 25 μL of complete RPMI 1640 was added to the ECM mix for a final volume of 152.25 μL and an MOI of 0.05. After mixing, 4 μL of the cell-laden ECM mix was added to each well in a PP device and allowed to gel at 37°C and 5% $CO_2$ for 2 h. After gelation, 8 μL of RPMI 1640 containing 15% HI-FBS and 25 mM HEPES was added atop each well and returned to the incubator. Media was changed daily for the entirety of the experiments. For all monoculture infection experiments (**Figures 2**, **3**), MDMs were stained with CellTracker Green CMFDA dye (Thermo Fisher Scientific) according to manufacturer's protocols. Briefly, MDMs were rinsed with 1X PBS, and 10 μM CellTracker Green in serum-free media was added for 30 min at 37°C, washed once with 1X PBS, and then incubated with complete media for 10 min prior to further processing or use. It is important to note that CellTracker Green CMFDA dye only stains live cells.

## 2D Angiogenesis Assay

Prior to seeding, PS Stacks devices containing a floor were chilled for 5 min at −80°C and then kept on ice for Matrigel seeding. 3 μL of Matrigel (8.6 mg/mL) was added to each well and devices rested on ice 30 min. The Matrigel was then polymerized for 30 min at 37°C. After polymerization, 3 μL of HUVECs were added atop the Matrigel for a final concentration of 1,650 cells per well ($5.5 \times 10^5$ cells/mL). Cells were allowed to adhere and self-assemble for 2 h at 37°C and 5% $CO_2$. Media was then aspirated and replaced with 2 μL of EGM-2 + 10% FBS coculture media.

To stack the layers, media was first removed from the model granuloma layers. Model granuloma layers were then placed atop the endothelial layers (containing 3 μL of media) and 7 μL of coculture media was placed atop each well of the stacked granuloma layers, to allow for feeding of both layers. Layers were separated by a thin layer of tape along the sides of the devices to ensure reproducible separation. Stacked devices were then placed in the incubator at 37°C and 5% $CO_2$. After 16 h, devices were inverted and separated, fixed with 4% paraformaldehyde for 30 min at 25°C, and stained as specified under Imaging. It is important to note that the self-assembled tubule network disassembles after 18–24 h of culture, therefore limiting the duration of the coculture experiment to within 2–18 h of seeding (Lonza, 2018); however, the modularity of this system enables users to combine layers at different time points (i.e., Day 2 p.i. to Day 3 p.i., etc.) to examine various temporal signaling profiles.

## Imaging

To validate granuloma layer formation within our platform, MDMs were prestained with CellTracker Green CMFDA dye prior to infection and seeding into the Stacks. For imaging, the Stacks platform was placed on a 50 mm x 75 mm glass coverslip (#260462, Ted Pella Inc., Redding, CA, United States) and placed into an OmniTray™ with a 45 mm x 70 mm rectangle cut out of the bottom. Fluorescent images were obtained on a Zeiss Axiovert 200 coupled with an Axiocam 503 mono camera (Carl Zeiss AG, Oberkochen, Germany). For confocal imaging, all wells were fixed with 4% paraformaldehyde for 1 h at 25°C and then covered with PBS; the same imaging protocol was then followed as above. Fluorescent confocal images were obtained on a Leica TCS SP5 II Laser Scanning Confocal Microscope (Leica Camera AG, Wetzlar, Germany), with a z-depth of 66.47 μm and step size of 1.01 μm. Images obtained with the Zeiss Axiovert 200 were analyzed with Fiji (ImageJ), and images obtained with the Leica TCS SP5 II were analyzed with Leica LAS X software (Leica).

For vasculature layer imaging, cells were permeabilized with 0.5% Triton-X 100 for 30 min and then stained with Phalloidin 488 (1:50) (Molecular Probe A12379) and Hoechst nuclear stain

(1:1000) (Molecular Probe H1399) overnight. After overnight incubation, cells were rinsed thrice with 0.2% Triton-X 100 for 10 min each and then covered with PBS for imaging. Devices were placed on a 75 mm × 50 mm glass coverslip (#260462, Ted Pella Inc., Redding, CA, United States) and placed in an Omnitray™ with a 45 mm × 70 mm rectangle cut out of the bottom. Fluorescent images were obtained on a Zeiss Axiovert 200 coupled with an Axiocam 503 mono camera (Carl Zeiss AG, Oberkochen, Germany). Images obtained were analyzed with Fiji (ImageJ).

## Angiogenesis Morphological Analysis

To analyze differences in morphology in the endothelial layer we used default functions of Image J (Fiji) to quantify the tubule index (perimeter/area ratio) (Theberge et al., 2015). The image analysis procedure is described in the methods and SI of Theberge et al. (2015), a summary is included here. For quantification, the 8-bit image containing the phalloidin channel (488) was selected and a threshold (Huang Dark) was applied to get the outline of the endothelial culture and saved (Image 1). The "Fill Holes" function was applied and saved (Image 2), and then Image 2 was subtracted from Image 1 to generate an image containing the holes/gaps in the endothelial morphology (Image 3). The total area of the phalloidin stain was then calculated by subtracting the area of Image 3 (holes) from Image 2 (fill holes), and the perimeter of the stain was calculated by adding the perimeter of Image 2 and Image 3. The area and perimeter were measured using the function "Analyze Particles," with the following parameters: size: 25-infinity (include pixel units), circularity: 0.00–1.00. The ImageJ macro for this process is included in the **Supplementary Material** and is based off the macro used in Yu et al. (2019).

Exclusion criteria for experimental artifacts that interfered with the imaging technique was developed to exclude wells unable to be analyzed with this technique. For example, if a collagen plug from the model granuloma layer detached and fell into a endothelial layer well during separation of the layers, the endothelial morphology was obscured by signal from the MDMs in the collagen plug and therefore unable to be accurately measured. All images were assigned a randomized code and individuals not involved in the project determined which images to exclude base on established criteria. Images were then analyzed according to the measurement protocol above.

## Cytokine Analysis

Cytokine analyses were performed with a custom Luminex ProcartaPlex multiplex assay for IL-6, TNFα, and VEGF (Thermo Fisher Scientific). Supernatant samples were collected and pooled from a single device ($n$ = 24 wells, 8 μL/well) during daily media changes and stored at −80°C until use. Samples were collected from the same device over a 5-day period, such that each sample contains cytokines secreted within 24 h of collection (i.e., Day 2 p.i. cytokine levels indicate what was secreted between Day 1 and Day 2 p.i., etc.). In order to ensure sufficient volume of supernatant for analysis with the Luminex multiplex assay (50 μL), samples were pooled across individual wells; while this volumetric limitation is linked to the specific readout we selected, alternative analyses such as mRNA analysis (Yu et al., 2019) or intracellular cytokine staining can be applied to the cells within a single well. For analysis, samples were thawed on ice and analyzed according to the manufacturer's protocols for Luminex multiplex assays. Samples were analyzed on a Luminex 100/200 System instrument with xPONENT software (Fred Hutchinson Cancer Center Core Facility). All results were analyzed and visualized using Prism 7 software (GraphPad Software, San Diego, CA, United States).

# DATA AVAILABILITY STATEMENT

The raw data supporting the conclusions of this article will be made available by the authors, without undue reservation.

# AUTHOR CONTRIBUTIONS

SB and AT conceived of the project. SB and MG performed all experiments and data analysis and wrote the manuscript. XS, CS, and AT advised the project and edited, revised, and provided feedback on the manuscript. All authors reviewed and approved the final manuscript.

# FUNDING

We acknowledge the support of the Biochemical Diagnostics Foundry for Translational Research supported by the M. J. Murdock Charitable Trust. This work was supported by NIH R35GM128648, the University of Washington, the Mary Gates Endowment, and by the National Science Foundation Graduate Research Fellowship Program under Grant No. DGE-1256082 (SB). Any opinions, findings, and conclusions or recommendations expressed in this material are those of the author(s) and do not necessarily reflect the views of the National Science Foundation.

# ACKNOWLEDGMENTS

We would like to thank Dr. Shahin Shafiani (Urdahl Lab) for providing the mCherry *Mycobacterium bovis* BCG strain, Dr. Jason Yu for providing help on the Stacks platform, Tammi van Neel and Tianzi Zhang for image review, Ashley Dostie for obtaining the Stacks image, and Erik Layton (Seshadri Lab) for PBMC isolation training.

# SUPPLEMENTARY MATERIAL

The Supplementary Material for this article can be found online at: https://www.frontiersin.org/articles/10.3389/fbioe.2020.00931/full#supplementary-material

## REFERENCES


Berry, M. P. R., Graham, C. M., McNab, F. W., Xu, Z., Bloch, S. A. A., Oni, T., et al. (2010). An interferon-inducible neutrophil-driven blood transcriptional signature in human tuberculosis. *Nature* 466, 973–977. doi: 10.1038/nature09247

Berthier, E., Dostie, A. M., Lee, U. N., Berthier, J., and Theberge, A. B. (2019). Open microfluidic capillary systems. *Anal. Chem.* 91, 8739–8750. doi: 10.1021/acs.analchem.9b01429

Bielecka, M. K., Tezera, L. B., Zmijan, R., Drobniewski, F., Zhang, X., Jayasinghe, S., et al. (2017). A bioengineered three-dimensional cell culture platform integrated with microfluidics to address antimicrobial resistance in tuberculosis. *mBio* 8:e02073-16. doi: 10.1128/mBio.02073-16

Birkness, K. A., Guarner, J., Sable, S. B., Tripp, R. A., Kellar, K. L., Bartlett, J., et al. (2007). An in vitro model of the leukocyte interactions associated with granuloma formation in *Mycobacterium tuberculosis* infection. *Immunol. Cell Biol.* 85, 160–168. doi: 10.1038/sj.icb.7100019

Bishop, E. T., Bell, G. T., Bloor, S., Broom, I. J., Hendry, N. F. K., and Wheatley, D. N. (1999). An in vitro model of angiogenesis: basic features. *Angiogenesis* 3, 335–344. doi: 10.1023/A:1026546219962

Casavant, B. P., Berthier, E., Theberge, A. B., Berthier, J., Montanez-Sauri, S. I., Bischel, L. L., et al. (2013). Suspended microfluidics. *PNAS* 110, 10111–10116. doi: 10.1073/pnas.1302566110

Cronan, M. R., Matty, M. A., Rosenberg, A. F., Blanc, L., Pyle, C. J., Espenschied, S. T., et al. (2018). An explant technique for high-resolution imaging and manipulation of mycobacterial granulomas. *Na. Methods* 15, 1098–1107. doi: 10.1038/s41592-018-0215-8

Cronan, M. R., and Tobin, D. M. (2014). Fit for consumption: zebrafish as a model for tuberculosis. *DMM Dis. Models Mech.* 7, 777–784. doi: 10.1242/dmm.016089

Crouser, E. D., White, P., Caceres, E. G., Julian, M. W., Papp, A. C., Locke, L. W., et al. (2017). A novel in vitro human granuloma model of sarcoidosis and latent tuberculosis infection. *Am. J. Respir. Cell Mol. Biol.* 57, 487–498. doi: 10.1165/rcmb.2016-0321OC

Darboe, F., Mbandi, S. K., Naidoo, K., Yende-Zuma, N., Lewis, L., Thompson, E. G., et al. (2019). Detection of tuberculosis recurrence, diagnosis and treatment response by a blood transcriptomic risk signature in HIV-infected persons on antiretroviral therapy. *Front. Microbiol.* 10:1441. doi: 10.3389/fmicb.2019.01441

Datta, M., Via, L. E., Kamoun, W. S., Liu, C., Chen, W., Seano, G., et al. (2015). Anti-vascular endothelial growth factor treatment normalizes tuberculosis granuloma vasculature and improves small molecule delivery. *Proc. Natl. Acad. Sci. U.S.A.* 112, 1827–1832. doi: 10.1073/pnas.1424563112

Deb, C., Lee, C. M., Dubey, V. S., Daniel, J., Abomoelak, B., Sirakova, T. D., et al. (2009). A novel in vitro multiple-stress dormancy model for *Mycobacterium tuberculosis* generates a lipid-loaded, drug-tolerant, dormant pathogen. *PLoS One* 4:6077. doi: 10.1371/journal.pone.0006077

Domingo-Gonzalez, R., Prince, O., Cooper, A., and Khader, S. A. (2016). Cytokines and chemokines in *Mycobacterium tuberculosis* infection. *Microbiol. Spectr.* 4, 1–37. doi: 10.1128/microbiolspec.tbtb2-0018-2016

Elkington, P., Lerm, M., Kapoor, N., Mahon, R., Pienaar, E., Huh, D., et al. (2019). In vitro granuloma models of tuberculosis: potential and challenges. *J. Infect. Dis.* 219, 1858–1866. doi: 10.1093/infdis/jiz020

Engele, M., Stößel, E., Castiglione, K., Schwerdtner, N., Wagner, M., Bölcskei, P., et al. (2002). Induction of TNF in human alveolar macrophages as a potential evasion mechanism of virulent *Mycobacterium tuberculosis*. *J. Immunol.* 168, 1328–1337. doi: 10.4049/jimmunol.168.3.1328

Foreman, T. W., Mehra, S., Lackner, A. A., and Kaushal, D. (2017). Translational research in the nonhuman primate model of tuberculosis. *ILAR J.* 58, 151–159. doi: 10.1093/ilar/ilx015

Gern, B., Plumlee, C., Gerner, M., and Urdahl, K. (2017). Investigating immune correlates of protection to tuberculosis using an ultra-low dose infection in a mouse model. *OFID* 4(Suppl. 1), 47–48.

Guyot-Revol, V., Innes, J. A., Hackforth, S., Hinks, T., and Lalvani, A. (2006). Regulatory T cells are expanded in blood and disease sites in patients with tuberculosis. *Am. J. Respir. Crit. Care Med.* 173, 803–810. doi: 10.1164/rccm.200508-1294OC

Harding, J. S., Herbath, M., Chen, Y., Rayasam, A., Ritter, A., Csoka, B., et al. (2019). VEGF-A from granuloma macrophages regulates granulomatous inflammation by a non-angiogenic pathway during mycobacterial infection. *Cell Rep.* 27, 2119.e6–2131.e6. doi: 10.1016/j.celrep.2019.04.072

Humayun, M., Chow, C. W., and Young, E. W. K. (2018). Microfluidic lung airway-on-a-chip with arrayable suspended gels for studying epithelial and smooth muscle cell interactions. *Lab Chip* 18, 1298–1309. doi: 10.1039/c7lc01357d

Kapoor, N., Pawar, S., Sirakova, T. D., Deb, C., Warren, W. L., and Kolattukudy, P. E. (2013). Human granuloma in vitro model, for TB dormancy and resuscitation. *PLoS One* 8:e0053657. doi: 10.1371/journal.pone.0053657

Kaufmann, S. H. E. (2004). New issues in tuberculosis. *Ann. Rheumat. Dis.* 63(Suppl. 2), 50–56. doi: 10.1136/ard.2004.028258

Koh, W., Stratman, A. N., Sacharidou, A., and Davis, G. E. (2008). Chapter 5 in vitro three dimensional collagen matrix models of endothelial lumen formation during vasculogenesis and angiogenesis. *Methods Enzymol.* 443, 83–101. doi: 10.1016/S0076-6879(08)02005-3

Lin, P. L., Plessner, H. L., Voitenok, N. N., and Flynn, J. A. L. (2007). Tumor necrosis factor and tuberculosis. *J. Investigat. Dermatol. Sympos. Proc.* 12, 22–25. doi: 10.1038/sj.jidsymp.5650027

Lonza (2018). *Clonetics Endothelial Cell System Technical Information & Instructions*. 1–15. Avaliable online at: https://bioscience.lonza.com/lonza_bs/US/en/download/product/asset/29423 (accessed April 12, 2020).

Martinez, A. N., Mehra, S., and Kaushal, D. (2013). Role of interleukin 6 in innate immunity to *Mycobacterium tuberculosis* infection. *J. Infect. Dis.* 207, 1253–1261. doi: 10.1093/infdis/jit037

Myllymäki, H., Bäuerlein, C. A., and Rämet, M. (2016). The zebrafish breathes new life into the study of tuberculosis. *Front. Immunol.* 7:196. doi: 10.3389/fimmu.2016.00196

Oehlers, S. H., Cronan, M. R., Beerman, R. W., Johnson, M. G., Huang, J., Kontos, C. D., et al. (2017). Infection-induced vascular permeability aids mycobacterial growth. *J. Infect. Dis.* 215, 813–817. doi: 10.1093/infdis/jiw355

Oehlers, S. H., Cronan, M. R., Scott, N. R., Thomas, M. I., Okuda, K. S., Walton, E. M., et al. (2015). Interception of host angiogenic signalling limits mycobacterial growth. *Nature* 517, 612–615. doi: 10.1038/nature13967

Ogongo, P., Steyn, A. J. C., Karim, F., Dullabh, K. J., Awala, I., Madansein, R., et al. (2020). Differential skewing of donor-unrestricted and γδ T cell repertoires in tuberculosis-infected human lungs. *J. Clin. Investigat.* 130, 214–230. doi: 10.1172/JCI130711

Ong, L. J. Y., Ching, T., Chong, L. H., Arora, S., Li, H., Hashimoto, M., et al. (2019). Self-aligning Tetris-Like (TILE) modular microfluidic platform for mimicking multi-organ interactions. *Lab Chip* 19, 2178–2191. doi: 10.1039/c9lc00160c

Osherov, N., and Ben-Ami, R. (2016). Modulation of host angiogenesis as a microbial survival strategy and therapeutic target. *PLoS Pathog.* 12:e1005479. doi: 10.1371/journal.ppat.1005479

Parasa, V. R., Muvva, J. R., Rose, J. F., Braian, C., Brighenti, S., and Lerm, M. (2017). Inhibition of tissue matrix metalloproteinases interferes with *Mycobacterium tuberculosis*-induced granuloma formation and reduces bacterial load in a human lung tissue model. *Front. Microbiol.* 8:2370. doi: 10.3389/fmicb.2017.02370

Parasa, V. R., Rahman, M. J., Hoang, A. T. N., Svensson, M., Brighenti, S., and Lerm, M. (2014). Modeling *Mycobacterium tuberculosis* early granuloma formation in experimental human lung tissue. *DMM Dis. Models Mech.* 7, 281–288. doi: 10.1242/dmm.013854

Peyron, P., Vaubourgeix, J., Poquet, Y., Levillain, F., Botanch, C., Bardou, F., et al. (2008). Foamy macrophages from tuberculous patients' granulomas constitute a nutrient-rich reservoir for *M. tuberculosis* persistence. *PLoS Pathog.* 4:e1000204. doi: 10.1371/journal.ppat.1000204

Polena, H., Boudou, F., Tilleul, S., Dubois-Colas, N., Lecointe, C., Rakotosamimanana, N., et al. (2016). *Mycobacterium tuberculosis* exploits the formation of new blood vessels for its dissemination. *Sci. Rep.* 6:33162. doi: 10.1038/srep33162

Puissegur, M. P., Botanch, C., Duteyrat, J. L., Delsol, G., Caratero, C., and Altare, F. (2004). An in vitro dual model of mycobacterial granulomas to investigate the molecular interactions between mycobacteria and human host cells. *Cell. Microbiol.* 6, 423–433. doi: 10.1111/j.1462-5822.2004.00371.x

Ramakrishnan, L. (2012). Revisiting the role of the granuloma in tuberculosis. *Nat. Rev. Immunol.* 12, 352–366. doi: 10.1038/nri3211

Russell, D. G., Cardona, P. J., Kim, M. J., Allain, S., and Altare, F. (2009). Foamy macrophages and the progression of the human tuberculosis granuloma. *Nat. Immunol.* 10, 943–948. doi: 10.1038/ni.1781

Sarkanen, J. R., Mannerström, M., Vuorenpää, H., Uotila, J., Ylikomi, T., and Heinonen, T. (2011). Intra-laboratory pre-validation of a human cell based in vitro angiogenesis assay for testing angiogenesis modulators. *Front. Pharmacol.* 1:147. doi: 10.3389/fphar.2010.00147

Saunders, B. M., and Britton, W. J. (2007). Life and death in the granuloma: immunopathology of tuberculosis. *Immunol. Cell Biol.* 85, 103–111. doi: 10.1038/sj.icb.7100027

Scanga, C. A., and Flynn, J. L. (2014). Modeling tuberculosis in nonhuman primates. *Cold Spring Harbor Perspect. Med.* 4:a018564. doi: 10.1101/cshperspect.a018564

Seitzer, U., and Gerdes, J. (2003). Generation and characterization of multicellular heterospheroids formed by human peripheral blood mononuclear cells. *Cells Tissues Organs* 174, 110–116. doi: 10.1159/000071151

Singh, P. P., and Goyal, A. (2013). Interleukin-6: a potent biomarker of mycobacterial infection. *SpringerPlus* 2, 2–9. doi: 10.1186/2193-1801-2-686

Su, X., Theberge, A. B., January, C. T., and Beebe, D. J. (2013). Effect of microculture on cell metabolism and biochemistry: do cells get stressed in microchannels? *Anal. Chem.* 85, 1562–1570. doi: 10.1021/ac3027228

Tezera, L. B., Bielecka, M. K., Chancellor, A., Reichmann, M. T., Shammari, B., Al Brace, P., et al. (2017). Dissection of the host-pathogen interaction in human tuberculosis using a bioengineered 3-dimensional model. *eLife* 6:e2128. doi: 10.7554/eLife.21283

Theberge, A. B., Yu, J., Young, E. W. K., Ricke, W. A., Bushman, W., and Beebe, D. J. (2015). Microfluidic multiculture assay to analyze biomolecular signaling in angiogenesis. *Anal. Chem.* 87, 3239–3246. doi: 10.1021/ac503700f

Torraca, V., Tulotta, C., Ewa Snaar-Jagalska, B., and Meijer, A. H. (2017). The chemokine receptor CXCR4 promotes granuloma formation by sustaining a mycobacteria-induced angiogenesis programme. *Sci. Rep.* 7, 18–20. doi: 10.1038/srep45061

World Health Organization (2019). *Global Tuberculosis Report*. Geneva: WHO.

Yong, K. S. M., Her, Z., and Chen, Q. (2018). Humanized Mice as Unique Tools for Human-Specific Studies. *Arch. Immunol. Ther. Exp.* 66, 245–266. doi: 10.1007/s00005-018-0506-x

Yu, J., Berthier, E., Craig, A., de Groot, T. E., Sparks, S., Ingram, P. N., et al. (2019). Reconfigurable open microfluidics for studying the spatiotemporal dynamics of paracrine signalling. *Nat. Biomed. Eng.* 3, 830–841. doi: 10.1038/s41551-019-0421-4

Zhan, L., Tang, J., Sun, M., and Qin, C. (2017). Animal models for tuberculosis in translational and precision medicine. *Front. Microbiol.* 8:717. doi: 10.3389/fmicb.2017.00717

**Conflict of Interest:** The authors acknowledge the following potential conflicts of interest in companies pursuing open microfluidic technologies: AT: Stacks to the Future, LLC.